Acta Biomaterialia xxx (xxxx) xxx

Contents lists available at ScienceDirect

Acta Biomaterialia

journal homepage: www.elsevier.com/locate/actbio

Full length article

Positive interactions of mechanical loading and PTH treatments on spatio-temporal bone remodelling

Vee San Cheong[a,b,*], Bryant C. Roberts[a,c], Visakan Kadirkamanathan[a,b], Enrico Dall'Ara[a,c]

[a] *Insigneo Institute for* in silico *Medicine, University of Sheffield, United Kingdom*
[b] *Department of Automatic Control and Systems Engineering, University of Sheffield, United Kingdom*
[c] *Department of Oncology and Metabolism, University of Sheffield, United Kingdom*

ARTICLE INFO

Article history:
Received 14 June 2021
Revised 3 September 2021
Accepted 17 September 2021

Keywords:
Bone remodelling
Micro-CT
Longitudinal imaging
In vivo loading
Parathyroid hormone
Osteoporosis

ABSTRACT

Osteoporosis is one of the most common skeletal diseases, but current therapies are limited to generalized antiresorptive or anabolic interventions, which do not target regions that would benefit from improvements to skeletal health. To improve the evaluation of treatment plans, we used a spatio-temporal multiscale approach that combines longitudinal *in vivo* micro-computed tomography (micro-CT) and *in silico* subject-specific finite element modeling to quantitatively map bone adaptation changes due to disease and treatment at high resolution. Our findings show time and region-dependent modifications in bone remodelling following one and two sets of mechanical loading and/or pharmacological interventions. The multiscale results highlighted that the distal section was unaffected by mechanical loading alone but the proximal tibia had the greatest gain from positive interactions of combined therapies. Mechanical loading abated the catabolic effect of PTH, but the main benefit of combined treatments occurred from the additive interactions of the two therapies in periosteal apposition. These results provide detailed insight into the efficacy of combined treatments, facilitating the optimisation of dosage and treatment duration in preclinical mouse studies, and the development of novel interventions for skeletal diseases.

Statement of Significance

Combined mechanical loading and pharmacotherapy have the potential to slow osteoporosis-induced bone loss but current therapies do not target the regions in need of strengthening. We show for the first time spatial region-dependant interactions between PTH and mechanical loading treatment in OVX mouse tibiae, highlighting local regions in the tibia that benefitted from separate and combined treatments. Combined experimental-computational analysis also detailed the lasting period of each treatment per location in the tibia, the extent of positive (or negative) interactions of the combined therapies, and the impact of each treatment on the regulation of bone adaptation spatio-temporally. This approach can be used to create hypothesis about the interactions of different treatments to optimise the design of biomaterials and medical interventions.

1. Introduction

The role of functional adaptation in protecting bone from fracture has been recognised since Julius Wolff linked the internal architecture of bones to stress trajectories [1]. This form-function relationship is achieved by the (re)modelling of bone tissue in response to external loads [2]. Further development through Frost's theory of "mechanostat' hypothesizes that the local strain environment mechano-regulates bone remodelling through a strain-controlled feedback loop, stimulating bone cell activity to remove excess bone in regions of low strain, and to form new bone in regions of high strain [3]. This knowledge has been used to treat bone diseases such as osteoporosis, through the prescription of exercises and whole-body vibration [4]. However, treatment based on mechanical loading alone has inherent risks as it may induce the very fracture that it is meant to prevent, as osteoporotic bones are low in bone mass and quality [4]. On the other hand, pharmacological treatments can strengthen the skeleton [5] and enhance bone's osteogenic response to loading [6]. However, anabolic agents are

* Corresponding author.
E-mail address: v.cheong@sheffield.ac.uk (V.S. Cheong).

https://doi.org/10.1016/j.actbio.2021.09.035

only approved by the US Food and Drug Administration for use in patients with severe osteoporosis up to a maximum 2 years [7]. Therefore, understanding how the regulation of (re)modelling is affected by mechanical loading and pharmacological treatment in preclinical investigations can improve the identification of effective treatment strategies for bone diseases.

Improvements in imaging techniques have enhanced our understanding of bone structural changes at different dimensional scales. However, the mechanisms underpinning the variation in spatial adaptation across the tibial length remain poorly understood [8,9], as most studies involving rodent long bones were performed on small regions of interests [6,10,11]. Standard analysis of sample regions in mice scanned using micro-computed tomography (micro-CT) includes the computation of morphometric (e.g. bone volume fraction, BV/TV, and trabecular thickness Tb.Th) and densitometric (e.g. bone mineral content, BMC) parameters as measures of bone health [12,13]. Studies have shown that 3D morphometric measurements highly correlate with the results from standard 2D histomorphometry, while overcoming limitations of the latter. Serial sectioning is destructive and limited to cross-sectional study design, requiring a larger sample size per study design; assessment of bone parameters is sensitive to the selection plane; fluorochrome labelling can only identify sites of apposition but it also alters mineral properties [12-14]. Contradictory results on the effects of bone anabolic treatments (specifically the injections of parathyroid hormone, PTH) in promoting bone health led to the development of spatio-temporal approaches based on longitudinal micro-CT imaging [15]. This approach has allowed the identification of early effects of combined pharmacological and mechanical treatments on the local densitometric properties in the entire mouse tibia [16]. However, most studies that investigated the effects of combined treatments utilised a cross-sectional study design in small segments of the bone [17], and have not quantified the spatio-temporal changes in morphometric and densitometric properties with treatment-induced shape changes [18]. Hence, a method to relate regions of bone adaptation across the bone length with modifications in bone shape is highly desirable to build predictive models of bone adaptation that can be used to test and optimise treatment strategies preclinically.

In vivo longitudinal imaging enables the monitoring of bone changes in intact whole bones of the same animals over time. Combined with dynamic 3D assessments with micrometre resolution, the lower inter-subject variation highlights the effects of novel treatments and reduces the number of animals required in the experiments. This is in line with 3Rs principles to refine, reduce and partially replace animals used in research [19]. The coupling of time-lapsed imaging with validated finite element analysis (FEA) [20-23] has advanced knowledge about the role of local mechanics in causing bone adaptation [18,24-27]. However, heterogenous spatio-temporal bone adaptation has been observed [8,18,24], and current methodologies have several limitations in correlating between bone adaptation and mechanical stimuli in animal models of osteoporosis. Firstly, current models average the computed strain across the cross-section [18,28,29] but the curvature of the mouse tibia varies up to ten times across the length of the tibia, affecting dramatically the strain in the different sectors of each section. Secondly, although previous studies have compared FE estimated strains with surface bone remodelling in subsections of the mouse tibia [10,30], little is known about what happens at the different active surfaces of the bone (endosteal and periosteal regions), and across different compartments (anterior, medial, posterior, lateral) in the whole bone due to oestrogen deficiency. Thirdly, it is not known if these models can be applied to evaluate the response of systemic changes due to diseases and pharmacological applications (e.g. oestrogen deficiency and PTH treatment) in the mouse tibia.

To overcome the above-mentioned challenges, we have combined multiscale longitudinal micro-CT and micro-FEA to precisely monitor and quantify changes in internal bone architecture and external geometry. We demonstrate for the first time the evolution of systemic and localised changes in terms of bone adaptation, densitometric and biomechanical properties following mechanical loading, PTH and combined treatments in the oestrogen deficient mouse tibia. The results address several unanswered questions in the preclinical assessment of bone health, including: (1) How long did the effect of each treatment persist and where within the tibia? (2) What is the role of geometry in the interaction between mechanical loading and PTH? (3) How does the regulation of bone adaptation change spatially and with time after treatment? Our results indicate for the first time the changing effectiveness of three treatment interventions in the oestrogen deficient mouse tibia with time. This improved understanding of the locations and nature of bone changes facilitaties the optimisation of treatment plans, dosage, and duration, in the clinical management of osteoporosis.

2. Methods

2.1. Animals

To evaluate the effect of disease and subsequent treatment across the tibial length, an optimised scanning protocol that minimised the effect of the ionising radiation on bone remodelling [31,32], for repeated imaging every 2 weeks, was performed on a mouse model of osteoporosis (Fig. 1A). The study design comprises of three treatment groups ($n = 6$ mice/group) after ovariectomy (OVX) – 1) mechanical loading (ML), 2) parathyroid hormone (PTH) and 3) concurrent mechanical and PTH (PTHML) treatments – and the untreated OVX control (UNT, $n = 5$) (Fig. 1B).

Eighteen healthy female C57BL/6 mice were obtained from Charles Rivers (Margate, UK) at 13-weeks of age. All animals were housed in a standard animal facility, with a 12 h light and 12 h dark cycle, controlled temperature of 22 °C, and fed ad libitum [16]. All animal procedures were conducted in compliance with the ARRIVE (Animal Research: Reporting of *in vivo* Experiments) guidelines, the UK Animals (Scientific Procedures) Act 1986 and were approved by the local Research Ethics Committee of the University of Sheffield. All animals were ovariectomised (OVX) at 14-weeks of age to induce bone loss due to oestrogen deficiency and mimic the effect of osteoporosis. The mice were randomised into 3 weight-matched groups ($n = 6$ per group) to receive parathyroid hormone treatment (PTH), mechanical loading treatment (ML), or combined PTH and mechanical loading treatments (PTHML) (Fig. 1B). Body weight was measured once a week.

2.1.1. PTH treatment

From 18-weeks till 22-weeks of age, all mice in this group were treated with 100μg/kg/day of parathyroid hormone (PTH1–34, Bachem, Bubendorf, Switzerland) by intraperitoneal injection 5 days a week.

2.1.2. In vivo mechanical loading

The loading procedure was based on an approach that was found to engender compressive and tensile strains of up to -1500 $\mu\varepsilon$ and 2000 $\mu\varepsilon$, respectively, in 12-weeks old tibia [33]. Mechanical loading was applied *in vivo* at 19- and 21-weeks with a 2–12 N trapezoidal load, 40 cycles/day and 3 days/week on alternate days to the right tibia fixed between two soft cups, as previously reported [16,24]. Each loading cycle was separated by a 10 s interval, loaded to a peak load of 12 N at 16 kN/s on a static 2.0 N preload, held for 0.2 s, before unloading at the same rate. Loading was conducted every other week from the *in vivo* scans to improve animal

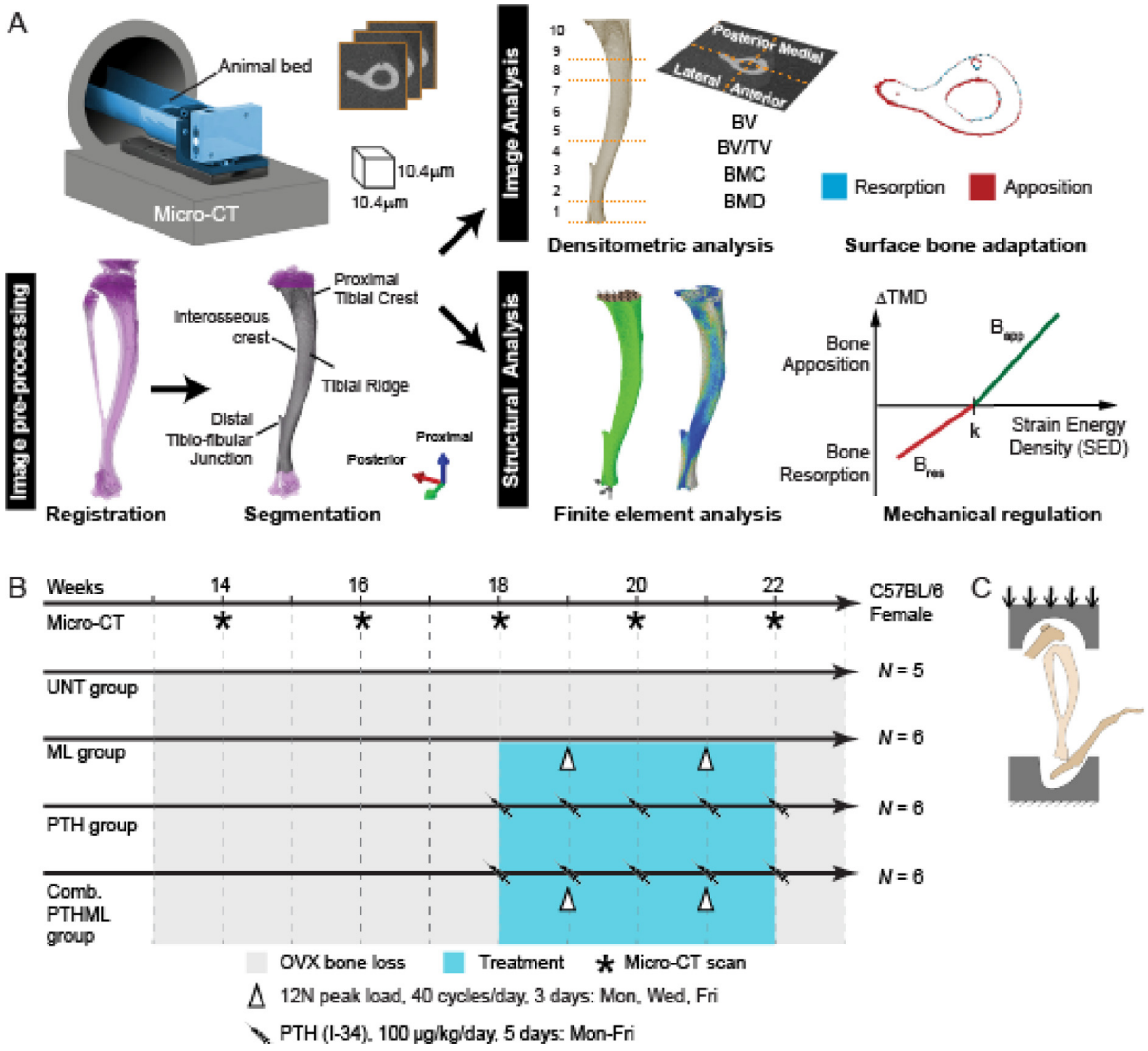

Fig. 1. Experimental design and data analysis for *in vivo* longitudinal micro-CT imaging. (A) Schematic of the pre-processing, image analysis and structural analysis workflow after the reconstruction of micro-CT scans. (B) Experimental study design investigating the effects of different treatments on bone health. ML: mechanical loading, PTH: parathyroid hormone treatment, PTHML: combined ML and PTH treatments, UNT: untreated OVX control. (C) The tibial loading model used.

welfare by minimising the number of anaesthesia sessions applied in the same week. All mice received intraperitoneal injection of vehicle 5 days/week.

2.1.3. Combined PTH and mechanical loading

The effects of combined mechanical loading and PTH treatments were investigated by administrating PTH 2–3 h post-loading. The procedures for PTH and mechanical loading are as stated in Section 2.1.1 and 2.1.2, respectively.

2.1.4. Untreated OVX control

To determine the lasting effect of treatment, all results were compared against a previous dataset which has the same scanning protocol as in this study, where the mice received no treatment after OVX at 14-weeks of age (UNT) [34].

2.2. In vivo *micro-CT monitoring of bone adaptation*

In vivo scanning of the whole right tibiae were performed every two weeks from week 14 until week 22 (vivaCT 80, Scanco Medical, Brüttisellen, Switzerland) with an optimised scanning procedure that offered the best compromise between scan quality and image acquisition time (100 ms integration time, 10.4 μm voxel size), while having minimal radiation effect on bone remodelling [31,32]. The X-ray source operated at 55 keV, 45 μA with a 0.5 mm aluminium filter, 750 projections/180° in a field of view of 32 mm to result in an isotropic voxel size of 10.4 μm at a nominal radiation dose of 256 mGy, to optimise between image quality and radiation dose [32]. All volumes were reconstructed using a third order polynomial beam hardening correction algorithm based on a 1200 mg HA/cm^3 phantom to minimise beam hardening artefacts [35].

2.3. 3D image registration

To compare bone changes within and between subjects, micro-CT images from all time points were rigidly registered to a reference bone (Amira 6.3.0, Thermo Fisher Scientific, France) using normalized mutual information as the optimization criterion and resampled using Lanczos interpolator [15,36] (Fig. 1A). Following geometrical alignment, a cropping plane perpendicular to the longitudinal axis was used to crop the images to 80% of the tibial length starting from the slice below the proximal growth plate, to exclude changes in the growth plate in the analysis [36]. The linear attenuation coefficient in each voxel was converted to tissue

mineral density (TMD) values using a five-rod densitometric phantom (Scanco Medical, Brüttisellen, Switzerland) and density calibration constants provided by the micro-CT manufacturer. The images were segmented by applying a threshold binarization, calculated as the midpoint of the background and object peaks in the grey value histograms [32].

2.4. 3D densitometric and spatial analyses

To quantify the regions of bone adaptation, densitometric properties — bone volume (BV), bone volume fraction (BV/TV), bone mineral content (BMC) and volumetric bone mineral density (BMD) — were computed for all images as detailed previously [36]. TV is the volume enclosed by the periosteal surface. The BMC of a region is the product of the voxel volume and the summation of the TMD of the bone voxels. BMD is computed by normalising BMC with TV. Quantification of the registration protocol achieved precision errors of less than 3.5% and intraclass correlation coefficients of over 0.8 in bone mineral content (BMC) [36], which enabled the comparison of the analysis results across mice and treatment groups. In addition, spatial analysis was conducted to identify the sites of bone remodelling, after superimposing the registered images of each mouse, aligning their volumetric centroid, and cropping them to the same length [24]. Surface voxels were determined by locating the endosteal and periosteal outlines of the segmented images, separated into regions that underwent increases (apposition) and decreases (resorption) in TMD values (Fig. 3A). The analyses were conducted for the whole bone and 40 compartments (10 longitudinal sections, 4 partitions in each section in the anterior, posterior, lateral and medial regions), which maximises the spatial resolution (number of longitudinal section) while ensuring measurement reproducibility (Matlab 2018a, MathWorks, MA, USA) [15,36]. All trabecular bone was found within section 10 of the longitudinal section and analysed together with the cortical bone.

2.5. Changes in strain distribution due to disease and treatment

Treatment-induced structural changes in the bones were assessed using micro-CT based finite element analysis (micro-FEA). Micro-FEA mesh were built by converting all bone voxels in the segmented images into linear hexahedral elements (Abaqus 2017, Dassault Systèmes, RI, USA). Tissue homogeneity was assumed, to isolate the changes in structural properties due to geometrical shape changes. This has been validated with *in situ* mechanical testing and digital volume correlation to reproduce the displacement and stiffness measured experimentally [21]. The predictions of the structural properties were also validated against monotonic experiments *ex vivo* [22,37]. Hence, all elements were assigned Young's modulus = 14.8 GPa and Poisson's ratio = 0.3 [21,22]. Micro-FEA was performed using a previously established protocol by applying a peak physiological load of 0.01355*BW N/g along the superior-inferior direction and 0.00289*BW N/g along the posterior-anterior direction, scaled according to the body weight (BW) of the mouse at each week [38]. This peak load was calculated from gait and force plate data acquired from mice during treadmill walking [39], and applied to the centroid of the most distal slice via kinematic coupling. The most proximal nodes were constrained from movement. Physiological loading, rather than the force applied during external loading, was applied to compare changes in the bone's ability to withstand physiological loading with time, following OVX and subsequent treatment(s). Strain Energy Density (SED) distributions were computed as the average for each slice, normalised against the tibial length. Statistical analyses were performed across SED distributions averaged across each section of the bone.

2.6. Mechanical regulation of bone adaptation

The local mechanical stimuli (SED) estimated from micro-FEA were used as inputs to a mechanoregulation algorithm to determine the extent that bone changes were linearly strain driven [38]. This bone adaptation algorithm is based on the mechanostat theory, which assumes that bone responds to changes in mechanical stimuli by linearly adapting its TMD [3]. This methodology has also been demonstrated to achieve high spatial match and predictive accuracy in apposition in OVX, healthy and mechanically loaded tibiae [24,38,40]. The mechanical stimuli were applied to bone geometries represented in the micro-CT images from week j to predict changes in bone geometry and to generate pseudo micro-CT images at week $j + 2$, for comparison with the experimental dataset [24,38]. The mechanoregulation algorithm has three model parameters (apposition/resorption remodelling rates and apposition-resorption threshold) that could be altered at the global level of the whole bone per animal, due to disease and treatment. Hence an optimisation algorithm that minimises the difference in the volumetric second moment between the geometries in the predicted and experimental images at week $j + 2$ was applied subject-specifically, to determine the remodelling parameters due to the treatment at week j:

$$\min\left(\sum_{i=1}^{10}\left(I_{xx,\,j+2}-I_{xx\ (predicted),\ j+2}\right)^2+\sum_{i=1}^{10}\left(I_{yy,\,j+2}-I_{yy\ (predicted),\ j+2}\right)^2\right)$$

Where the index j refers to the start of the time frame (week) of the input images used in computing the mechanical stimuli at week j and the predicted images at week $j + 2$. $I_{xx} = \iint y^2 dV$ and $I_{yy} = \iint x^2 dV$ are the volumetric second moment about the anterior-posterior and medial-lateral axis in each longitudinal section i of the tibia, respectively.

Comparisons of the accuracy in predicting the local bone changes, against the remodelling events computed from the follow-up images, were used to determine the extent that bone adaptation was mechanically strain driven at the organ level. Two spatial evaluation metrics were implemented by computing the total number of surface voxels that have the same state change (apposition or resorption) in the experimental and predicted datasets, 1) normalised by the total number of voxels with the state change in the predicted dataset (spatial match), or 2) normalised by total number of voxels with the state change in the experimental dataset (predictive accuracy). Spatial match and predictive accuracy are inverse measures of type I (false positive) and type II (false negative) errors, respectively. The evaluation metrics were computed separately for the endosteal and periosteal surfaces across 10 longitudinal sections of the tibia.

2.7. Statistical analyses

All results are presented as means ± standard deviation. Statistical analyses were performed using Origin 2019b (OriginLab Corp., MA, USA). Wilcoxon signed-rank test was used to assess between two time periods within each treatment group, while the Mann-Whitney U test was used when comparing between treatments at each time period due to the small sample size ($N = 5$ or $N = 6$). This was followed by two-way ANOVA to determine the effects of interactions if combined treatments were significantly different than both monotherapies and the changes were in the same direction. Where PTHML treatment was significantly different from the effect of a single monotherapy, the benefits are additive and no further statistical analysis was conducted. Regression analysis between SED and the frequency of bone remodelling across the most proximal seven longitudinal sections in the tibia (region proximal to the tibio-fibular joint) was performed using pooled data

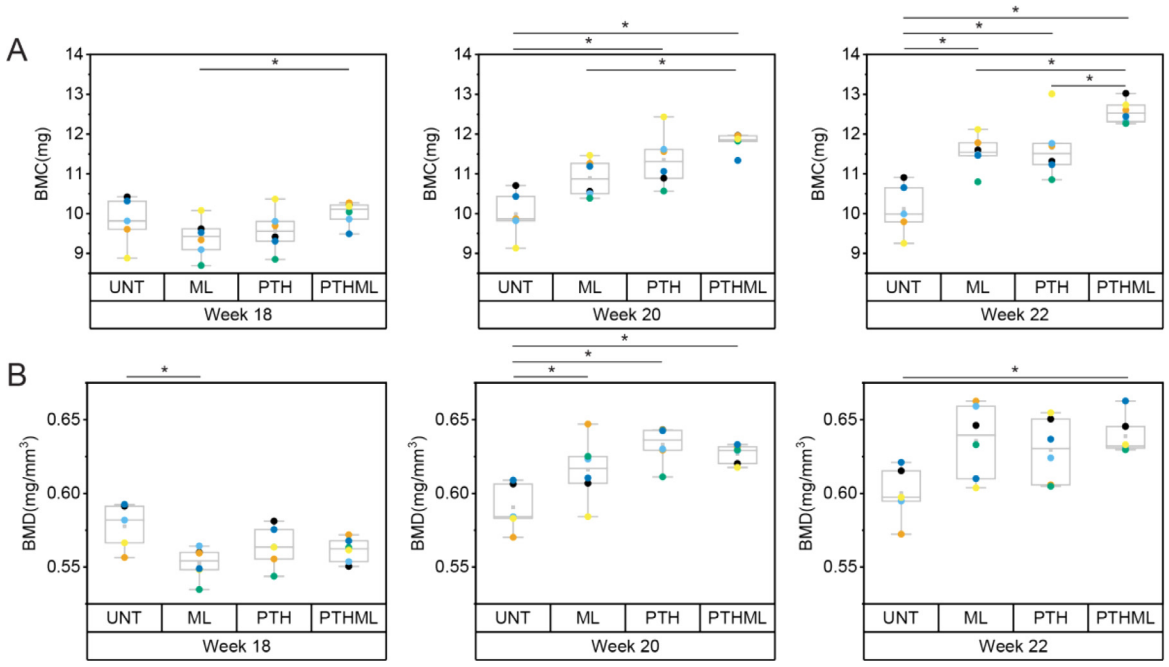

Fig. 2. Comparison of the benefits of mechanical loading (ML), parathyroid hormone (PTH) and combined treatments (PTHML) on densitometric parameters. The analyses were performed 2 and 4 weeks after the commencement of treatment at week 18, compared against the untreated OVX control (UNT). (A) Bone mineral content (BMC). (B) Bone mineral density (BMD). The boxes in the graphs encompass the 25th and 75th percentile (IQR); the whiskers indicate the range within 1.5 IQR. The horizontal bar and square box represent the median and mean, respectively. Data points (solid dots) identify the mice in the experiments ($N = 6$ for all treatment, $N = 5$ for UNT). * indicates significance ($p<0.05$; Mann-Whitney U test).

of all mice in each dataset. The F-test was used to compare the mechano-response between treatments. Statistical significance is indicated by $p< 0.05$ (two-tailed) and plotted in blue or orange in heat maps of p values.

3. Results

3.1. The lasting effect of treatment on bone properties

Analyses conducted in the whole bone showed that treatment by PTH or PTHML caused a significant increase in BMC and BMD, compared to the untreated OVX group at week 20 (Fig. 2A). ML treatment was only effective in improving BMD at week 20. At week 22, all treatment options were effective in increasing BMC compared to the UNT group, but only PTHML treatment significantly improved BMD. Although the results indicated a significant difference in BMC between ML and PTHML treated tibia at week 20, this was due to the initial difference in BMC at the commencement of treatment at week 18 (changes in BMC between weeks 18–20 were not significantly different: 16.1 ± 4.0% for the ML group; 18.6 ± 1.5% for the PTH group; 17.9 ± 1.5% for the PTHML group). At week 22, BMC in PTHML treated tibia was significantly higher than for other treatments, but the change in BMC at weeks 20–22 was not significantly different between ML and PTHML (ML: 6.0 ± 3.0%; PTH 2.6 ± 1.5%; PTHML: 6.5 ± 2.5%). Similar to BMC, the increase of BMD slowed between weeks 20–22. PTH was unable to prevent a reduction in BMD in some cases, and this change was significantly different to that in the ML group (ML: 3.2 ± 2.5%, PTH: −0.6 ± 2.0%, PTHML: 1.9 ± 2.1%) (Fig. 2B, Supplementary Fig. S1). Across the 4 weeks assessment period, only combined treatments (PTHML) resulted in significantly higher BMC and BMD than in nontreated tibiae at both weeks 20 and 22.

To quantify the sites of bone apposition and resorption every 2 weeks, image analysis was performed by superimposing and comparing the follow-up images. All three treatments were effective in increasing periosteal apposition and reducing periosteal resorption at weeks 18–20 and 20–22 for the most proximal 70% of the tibial length (Fig. 3A). However, a rebound in periosteal resorption at weeks 20–22 was observed for all treatments. The decrease in periosteal apposition at weeks 20–22 compared to weeks 18–20 was region-specific, affecting 10%, 80% and 50% of the sections for ML, PTH, and PTHML treatments, respectively. However, all the treatments had no significant effect on periosteal resorption for over 80% of the tibial length. The results also indicated that, apart from the distal region (Sections 1-2), there were no significant effect of all evaluated treatments in reducing endosteal resorption during the whole study period.

Understanding the changes in strain distribution in the mouse tibia under physiological loading is important to understand the relationship between the mechanical stimulus (e.g. the strain energy density, SED) and the bone adaptation. The micro-FEA results indicated that all three treatments were effective at reducing the SED across 90% of the tibia length 2 weeks after treatment commenced (week 20) (Fig. 3B). Reduction of SED slowed between weeks 20–22 across treatment in the cortical bone but increased for the region comprising primarily of trabecular bone (section 10). ML and PTHML induced similar patterns of region-specific strain changes; changes due to PTH were similar throughout the tibial length.

3.2. Interactions between mechanical loading and PTH are additive and competitive

For BMC, there was a similar effect of separate and combined mechanical loading and PTH treatments between weeks 18–20 except for section 9 of the medial sector (Fig. 4). Improvements in BMC at weeks 20–22 affected only the diaphysis and proximal tibia (Fig. 4F) and were lower than in weeks 18–20 (Fig. 4A). Between weeks 20–22, the changes in BMC were similar for the different sub-regions in the PTH group. The changes in BMC at week 22 due to PTHML treatment generally followed the trend observed in the ML group, with a similar trend for the changes in strain distribu-

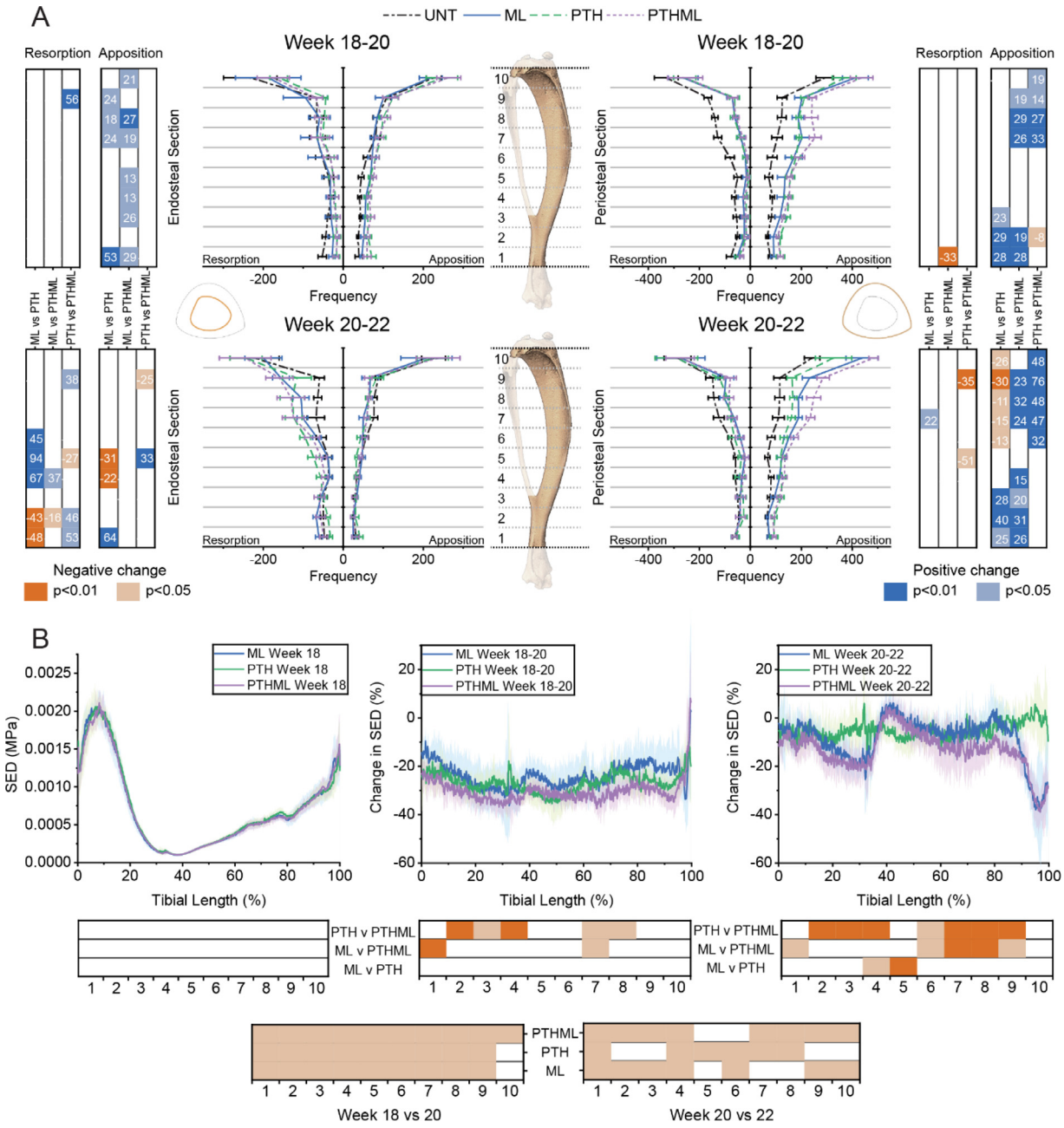

Fig. 3. The changes induced by mechanical loading (ML), parathyroid hormone (PTH) and combined treatments (PTHML) between weeks 18–20 and weeks 20–22. (A) Spatio-temporal differences in the experimentally measured bone adaptation on the endosteal and periosteal surfaces. (B) The changes in strain energy density (SED) along the tibial length show that regional improvements in bone adaptation benefitted the whole bone at weeks 18–20, but further reductions in SED were smaller or mixed (e.g. Section 5) at weeks 20–22. Statistical significant differences along the tibial length are represented as heat maps (Wilcoxon signed rank test). Numbers in the heat maps indicate the relative difference with respect to the treatment mentioned first.

tion (Fig. 3B). However, there was a reduction and improvement in BMC in the distal tibia for the ML and PTH groups, respectively, with PTH mitigating the effect of ML in the PTHML treated tibiae. These results showed that the benefits of combined ML and PTH treatments on the material and geometrical properties at week 20 were minimal across 80% of the tibia. At week 22, combined treatments improved BMC in the distal tibia and the structural properties in the proximal tibia non-additively, compared to separate individual treatments ($p<0.05$).

Periosteal apposition due to PTHML was significantly higher in the proximal tibia than either monotherapy at both weeks 18–20 and 20–22, indicating that there was a positive benefit of the combined treatments in the proximal tibia (Fig. 3A). In addition, there was a quantitative competitive relationship in increased periosteal apposition in section 9 at weeks 18–20 ($p = 0.01$). There was no significant interaction between PTH and ML in sections 7–8 at weeks 18–20, and sections 7–9 at weeks 20–22 ($p>0.05$). Endosteal resorption at the diaphysis (Section 4-6) was similar for all treatments at weeks 18–20. Endosteal resorption further increased following an additional 2 weeks of PTH monotherapy, indicating that the catabolic effect of PTH sets in after the second set of treatment. PTHML was able to abrogate some but not all the catabolic effect of PTH on the endosteum. For example, Section 5 in the diaphysis had significantly lower endosteum resorption for PTHML than PTH ($p<0.05$). PTHML also mitigated some of the bone loss in the distal tibia after ML at weeks 20–22. Periosteal apposition in the distal

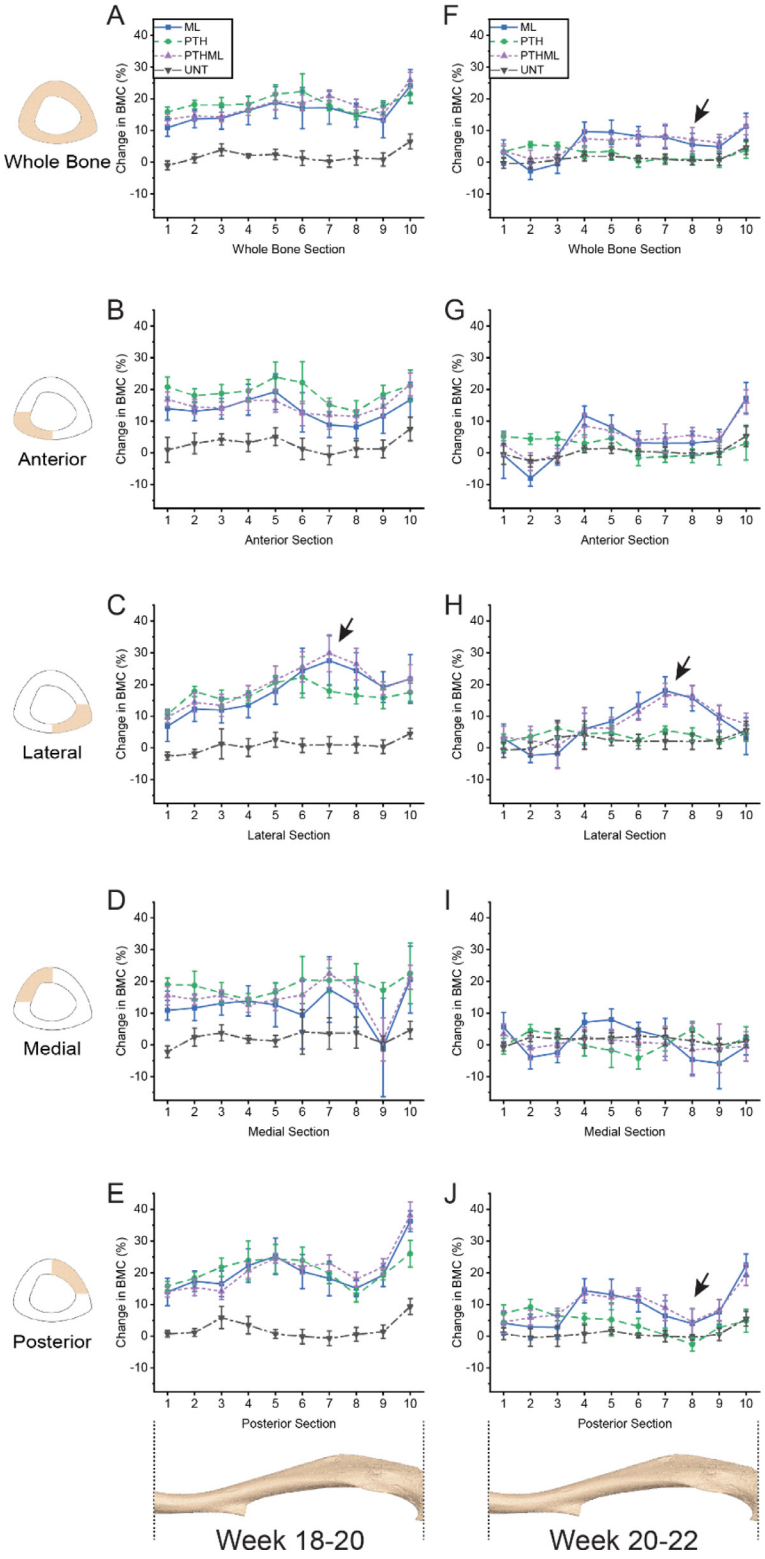

Fig. 4. The interactions between ML and PTH on the improvements to bone quality (BMC) compared with the untreated OVX mouse tibia (UNT). Lines indicate mean and standard deviation along the longitudinal axis from distal (1) to proximal (10) for (A-E) weeks 18–20 and (F-J) week 20–22 in the anterior, lateral, medial and posterior sections. The regional response induced by ML and PTHML were similar, indicating the dominant effect of mechanical loading on the proximal tibia. Arrows indicate sectors with a dominating ML effect on PTHML treatment.

tibia was not significantly different between PTH and PTHML treatments but were higher when compared with ML alone, indicating that combined effects were additive below the distal tibio-fibular joint.

3.3. Strain distribution predicted by the micro-FEA is correlated to local osteogenesis

Sub-analysis enables the examination of locations that were unaffected by the treatment strategy or may require further optimisation. Fig. 5 showed that the overall strain changes in the whole bone was driven by changes on the periosteal surface and the anterior region. Mechanical loading resulted in the smallest reductions in SED between weeks 18–20 in the anterior-medial region (Fig. 5 and Fig. 6). The results also showed some reversal in the initial reduction of SED in the proximal tibia (sections 8 and 9) at week 22 in the medial region for the ML and PTH treated groups. Visualisation of the locations of bone adaptation revealed that the increase in SED for all three treatments at week 22 was linked to the locations of increased resorption (Fig. 6). This increase in SED was mitigated by higher levels of bone apposition in the ML and PTHML groups, in contrast to the PTH group (Fig. 6F, I, L). The increase in bone apposition at both weeks 20 and 22 across treatments prevented the increase of SED that was observed in the untreated OVX tibia.

Combining image analysis and mechanical stimuli (i.e. the strain and SED fields) obtained from micro-FEA [38] enables the assessment of the effect of each treatment to withstand daily physiological loads. The correlation plots indicated a regional difference in bone adaptation across the different groups, with a significant correlation between the mechanical stimulus and the periosteal apposition for the most proximal 70% of the tibia, above the tibio-fibular joint at weeks 20–22 (F-test: $p<0.001$; $0.572<R^2<0.890$) (Fig. 7B). Conversely, no correlation was found for regions distal to the tibio-fibular joint (grey markers). At weeks 18–20, significant differences were found between the PTHML group and either monotherapy (F-test: $p<0.01$; $0.617<R^2<0.797$). All the three treatments triggered an effective anabolic response compared to the untreated OVX group at weeks 18–20 and 20–22 (F-test: $p<0.0001$). Mechanical loading-based treatments led to the highest increase in periosteal apposition rate, especially in the posterior regions (Fig. 7D, Supplementary Fig. S3). The response in each treated group was significantly different from each other at both time periods for all groups except between ML and PTH at weeks 18–20 (F-test: $p< 0.01$). On the contrary, induced periosteal resorption was similar for each treatment at either weeks 18–20 or 20–22 in the whole, anterior, or proximal tibia (Fig. 7C, E, Supplementary Fig. S3). Compared to the untreated OVX group, there was only a significant difference in periosteal resorption with the PTH group at weeks 20–22 (F-test: $p<0.05$).

3.4. Correlating tissue loading with predications of spatial bone adaptation

Micro-FEA modelling was coupled with a standard mechanostat algorithm [24] to investigate the effects of each treatment on the mechanical regulation of bone adaptation. Using an organ-level linear algorithm that accounts for the changes in bone curvature along the tibia, the results showed that all treatments followed a similar trend across the tibial length, with 50–90% of the bone apposition linearly related to physiological strain (Fig. 8). All parameters assigned to the mechanostat model, optimised to minimise the error between the predicted and actual volumetric second moment, can be found in Supplementary Table S1. The remodelling thresholds and the resorptions rates for the PTHML group were significantly different compared to either monotherapy at both weeks 18–20 and 20–22 ($p<0.05$). The lower prediction accuracy in periosteal apposition for the PTHML group suggests that it has a greater extent of bone apposition that was not linearly strain driven (Fig. 8). The higher spatial match for ML and PTHML groups than PTH suggests the higher dominance of mechanical regulation in mice that were treated with passive loading. The low prediction accuracy for resorption is probably the result of assuming an inverse correlation between SED and resorption as in the mechanostat theory; however the experimental results showed a direct relationship between resorption and SED (Fig. 7C, E). These results showed that the catabolic effects accompanied the treatment-induced anabolic effects as part of the remodelling cycle. Hence, resorption is not mechanically regulated but it is probably driven by biological stimuli at the cell-tissue level.

4. Discussion

Results from recent longitudinal studies indicate that mechanical loading treatment exerts spatial differences in the retention of accrued benefits in the whole bone of healthy [18] and OVX [24] mouse tibia. Enhancement of this natural anabolic stimulus with systemic anabolic PTH treatment has shown mixed site-specific effects in small segments of the healthy tibia [6,11] and across whole OVX tibiae for morphometric and densitometric parameters [16]. Hence, it is imperative to develop a detailed understanding of the modulation of mechanical and pharmacological treatment on bone adaptation across length scale and time in order to optimise the treatment of osteoporosis.

Many studies that investigated the osteogenic response of mechanical loading and pharmacological treatments were conducted using a cross-sectional study design involving specific segments of the mouse tibia [6,11]. Longitudinal imaging has several advantages in monitoring bone changes with time compared to traditional methods, including the reduction of inter-subject differences, measurement variability and sample size required. However, the applicability of this approach to evaluate the mechanisms of actions of individual and combined treatments at improving skeletal health in the whole diseased tibia has not been evaluated. The results showed for the first time that combined *in vivo* micro-CT imaging and *in silico* modelling enable the assessment of the efficacy of novel treatments to osteoporosis in three distinct aspects in 4D (time and space). Firstly, we quantified the benefits of each monotherapy in slowing the progression of accelerated bone resorption due to OVX spatio-temporally, and delineated that most of the positive interactions between mechanical loading and PTH treatment were additive. Secondly, the link between the locations of bone adaptation and the local stimuli under physiological loading was investigated to determine the contribution of apposition and resorption on each bone surface in improving bone health. Thirdly, we investigated the changes in the mechanical regulation of bone remodelling after two and four weeks of treatment to withstand daily physiological loading.

The results indicated that all three treatments had similar early benefits to densitometric properties at weeks 18–20 across the tibial length through elevated rates of bone apposition and reduced rates of resorption, but slowed at weeks 20–22 with continued treatment. Although the lower bone apposition of the ML group at weeks 20–22 is consistent with earlier studies that loaded the healthy tibia [18], the change in BV/TV of all three treatments at the later period is in contrast with the treated OVX caudal vertebrae [25]. Previous studies have typically focussed on standard morphometric analysis [10,25,33,41] or spatial distribution of bone remodelling [8,42], but our results showed for the first time that the smaller changes at weeks 20–22 than 18–20 are linked to the rebound in periosteal resorption and the reduction in apposition. In particular, the even changes in periosteal remodelling for PTH

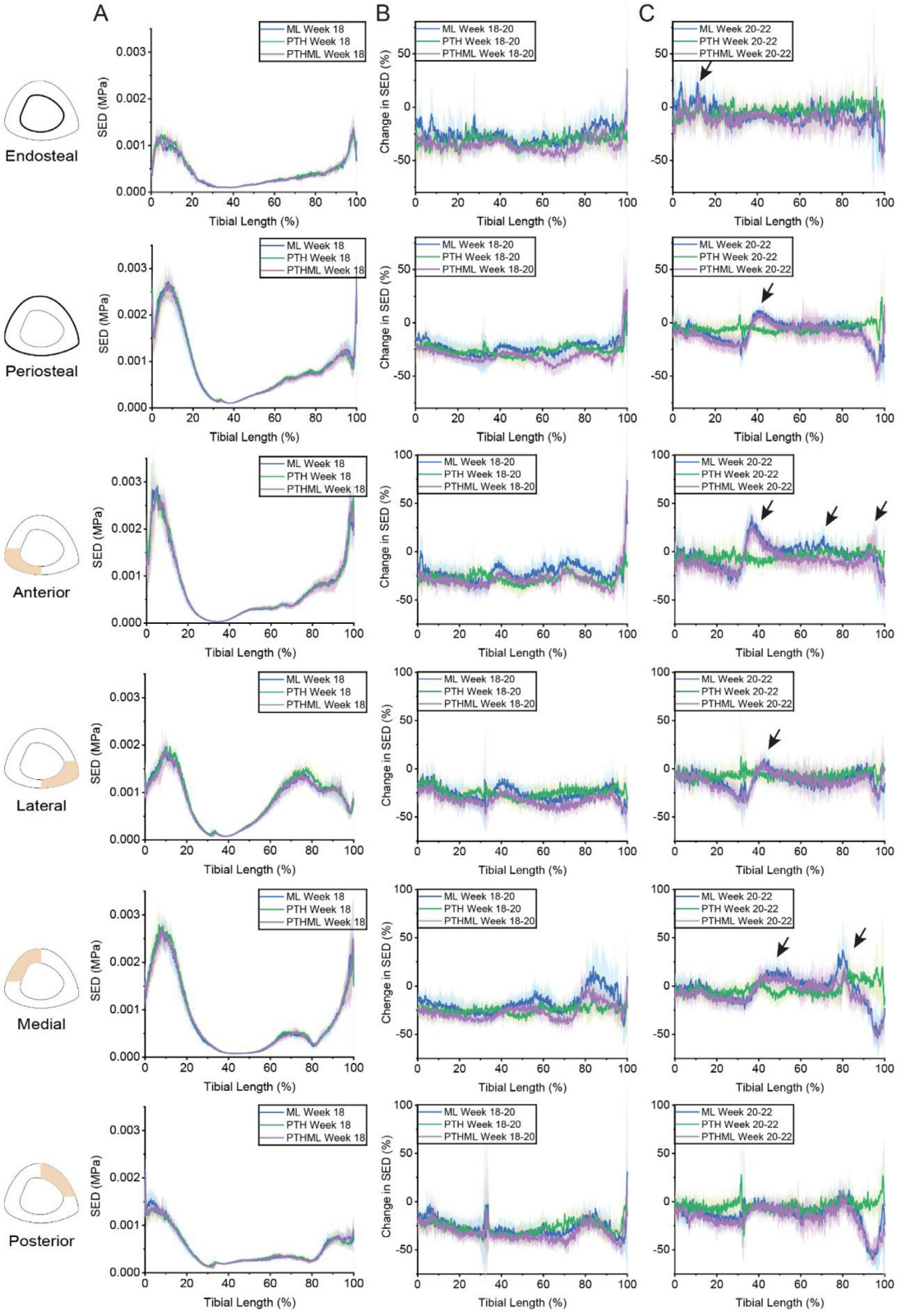

Fig. 5. Spatio-temporal changes in strain energy density (SED) for ML, PTH and ML treatments with time. The results show that bone adaptation on the anterior and posterior regions contributed predominately to the overall changes in SED. (A) SED frequency distribution plot at the commencement of treatment at week 18. Effect of increasing the period of treatment in terms of changes in SED at (B) weeks 18–20 and (C) weeks 20–22. All values average ± standard deviations. Arrows indicate a reversal from the initial reduction in SED.

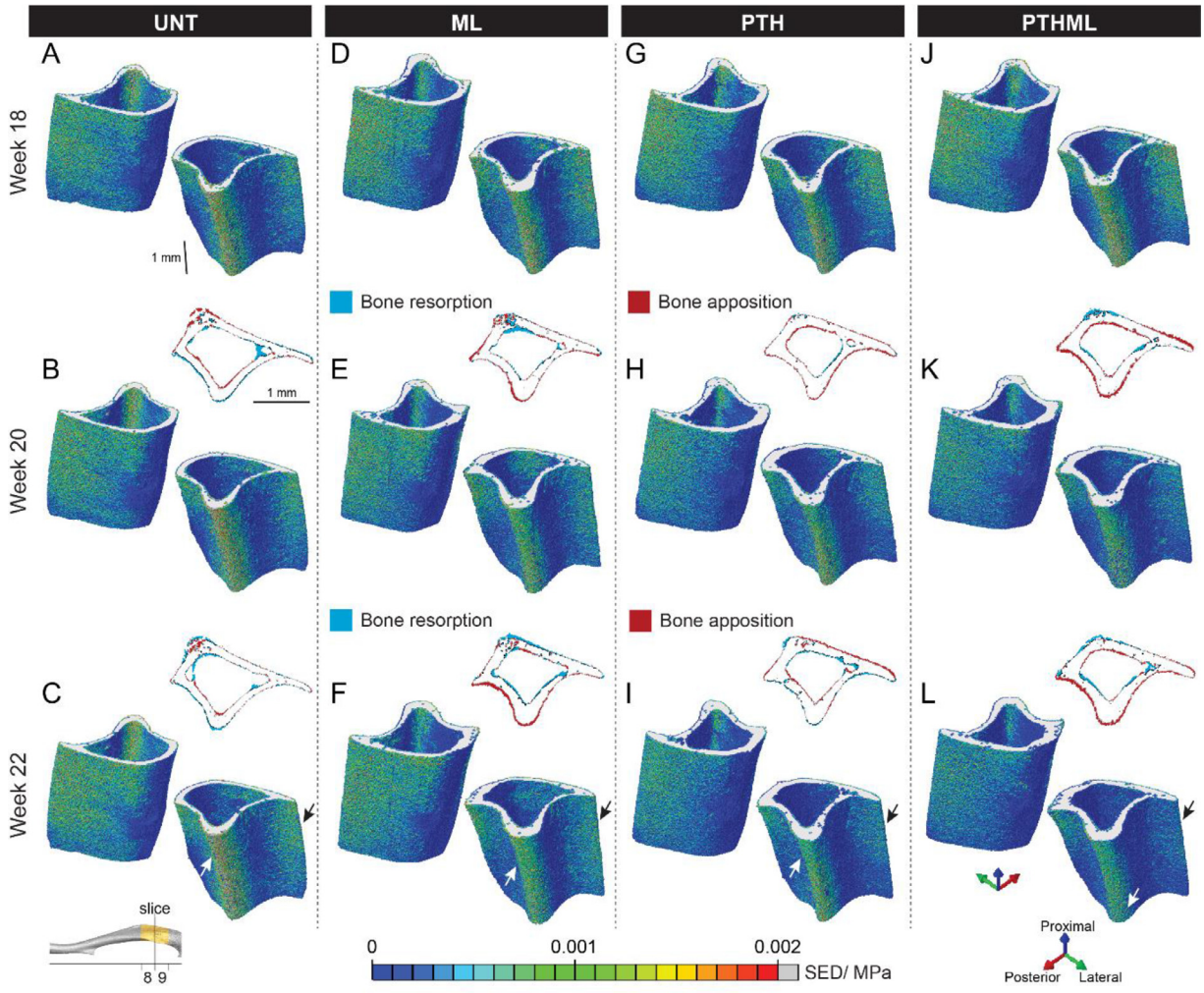

Fig. 6. Bone adaptation and changes in mechanical environment in control and treated tibiae. 3D views show the decrease in strain energy density (SED) distribution in the proximal tibia (section 8–9) under physiological loading between weeks 18–20 in the treated groups, and some loss of the accrued benefits in week 22. (A-C) UNT, (D-F) ML, (G-I) PTH and (J-L) PTHML. 2D slices in between the weeks show the locations of bone adaptation in the mid-section. White arrows indicate regions with increases in SED between weeks 20–22. Black arrows indicate regions with the largest difference between treatment groups.

across the tibial length at weeks 20–22 (Fig. 3A) were reflected in the even increase in SED (Fig. 3B) and matched by the large drop off in the rate of change of densitometric properties across the tibial length (Fig. 4, Supplementary Fig. S2). Although bone adaptation was similar for ML and PTH monotherapies across over 50% of the tibial length at weeks 18–20, loading-induced benefits targeted primarily the proximal region at weeks 20–22, consistent with loading studies conducted on healthy tibia [11]. At weeks 20–22, the majority of the earlier accrued benefits at the distal region (Section 1-3) were lost in tibiae treated with mechanical loading alone, resulting in higher SED in the endosteal section (Fig. 5A). Morphometric parameters of both ML and PTHML groups were similar or higher than data from wild type negative control at both weeks 20 and 22 [16,34]. However, from the spatial (Fig. 3) and micro-FE analyses (Fig. 6, Fig. 7), the higher apposition and lower resorption of PTHML at both time periods across the tibial length made it more effective than either monotherapy in slowing the progress of osteoporosis at week 22.

Assessment of the amount and rate of bone adaptation revealed that PTH and mechanical loading's enhancement of each other is time- and site- dependant (Fig. 3A). Mechanical loading had a slight dominating effect at weeks 18–20 due to similarities with PTHML treatment for the SED curve at the organ level (Fig. 3B) and BMC in the lateral compartment (Fig. 4C). However, this effect became stronger at weeks 20–22 with close similarities in the ML- and PTHML- induced BMC and SED changes in all four sectors at the tissue level (Fig. 4,Fig. 5). This disparity could be due to the strong anabolic effect of PTH at the earlier period of weeks 18–20, as reported in the OVX caudal vertebra [25], healthy femur and tibia [11,43]. Strong anabolic response are observed during the 'anabolic window' when PTH stimulates bone apposition without an increase in resorption [44,45]. However, the results showed that the window passed after week 20, as the increase in resorption led to an overall increase in SED and reduction in BMC at weeks 20–22 in the PTH treated tibiae. Fig. 3A showed that mechanical loading had a small effect in abrogating the catabolic effects of PTH at weeks 20–22, but improvements in BMC and strain distribution (Fig. 3B, Fig. 4) occurred from the positive interactions of the two therapies in periosteal apposition.

The results also showed that PTH's enhancement of mechanical loading was largely additive. A competitive response was seen only in section 9 of the tibia at weeks 18–20 (Fig. 3A), where the effect of the combined PTHML treatment was statistically smaller than the sum of the effects of the monotherapies. However, the impact of the benefits of combined treatment on strain distribution in the proximal tibia at week 22 was non-additive ($p<0.05$) (Fig. 3B). Previous studies have shown the synergistic effect of PTH and mechanical loading in the proximal tibia in healthy, young 19

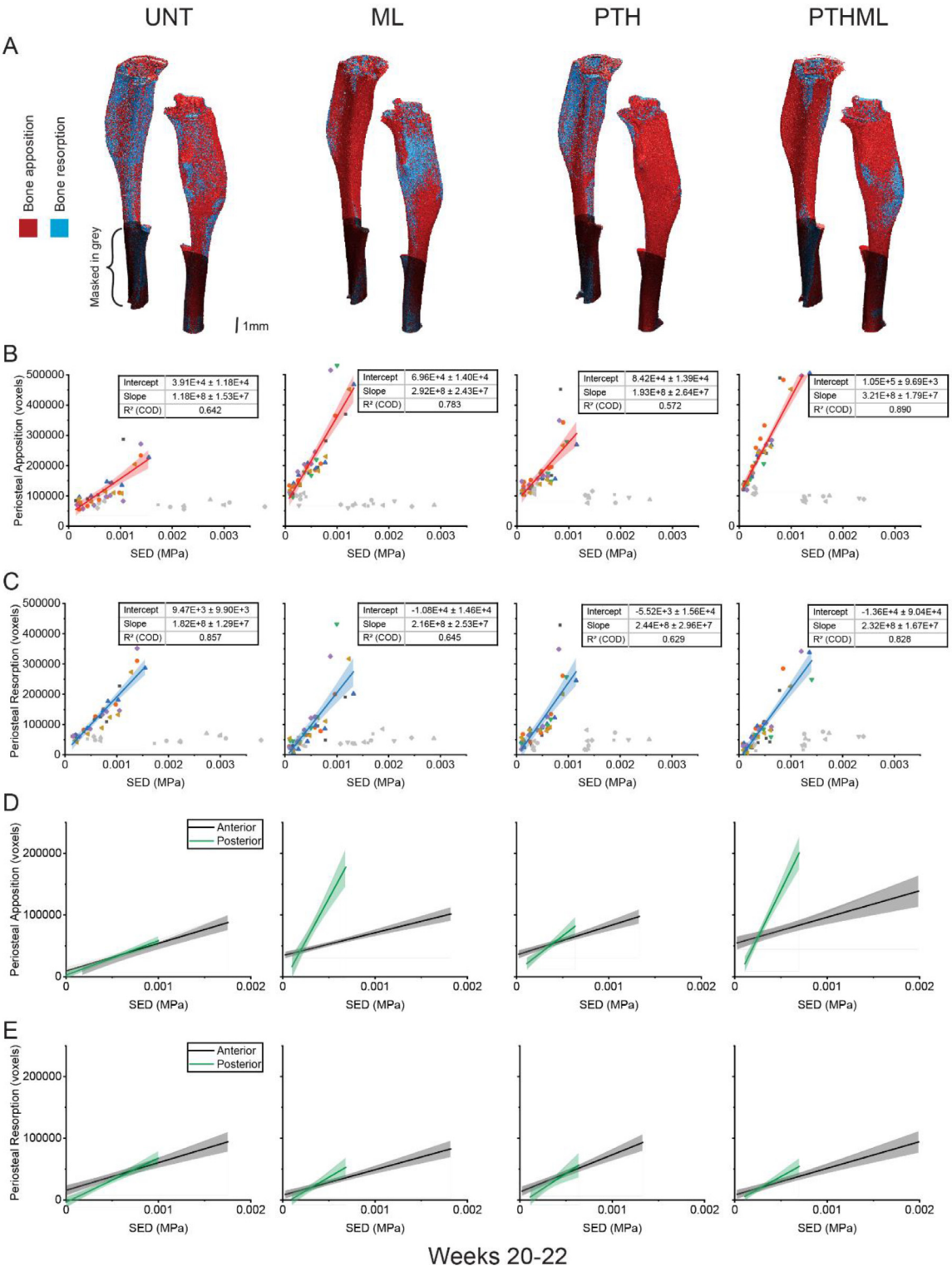

Fig. 7. The link between local mechanical stimulus and bone adaptation. Correlations between bone adaptation between weeks 20–22 and SED from the preceding week 20 show the efficacy of each treatment on the mouse tibia is region-dependant. (A) Locations and extent of bone adaptation for representative tibiae from each treatment group. The graphs show individual measurements of bone adaptation, across the 10 sections for each animal. Regression results and the 95% confidence interval in the most proximal seven sections of the whole bone for (B) periosteal apposition (C) and periosteal resorption. (D) Anabolic effect of mechanical loading was highest in the posterior region. (E) The regional effect on periosteal resorption was minimal for all treatments. Coloured dots represent the data at each of the 10 longitudinal sections of the mouse tibia, pooled together for all mice ($N = 6$ for all treatment groups, $N = 5$ for UNT). Dots in grey are from sections below the tibio-fibular joint and not used in the regression analysis.

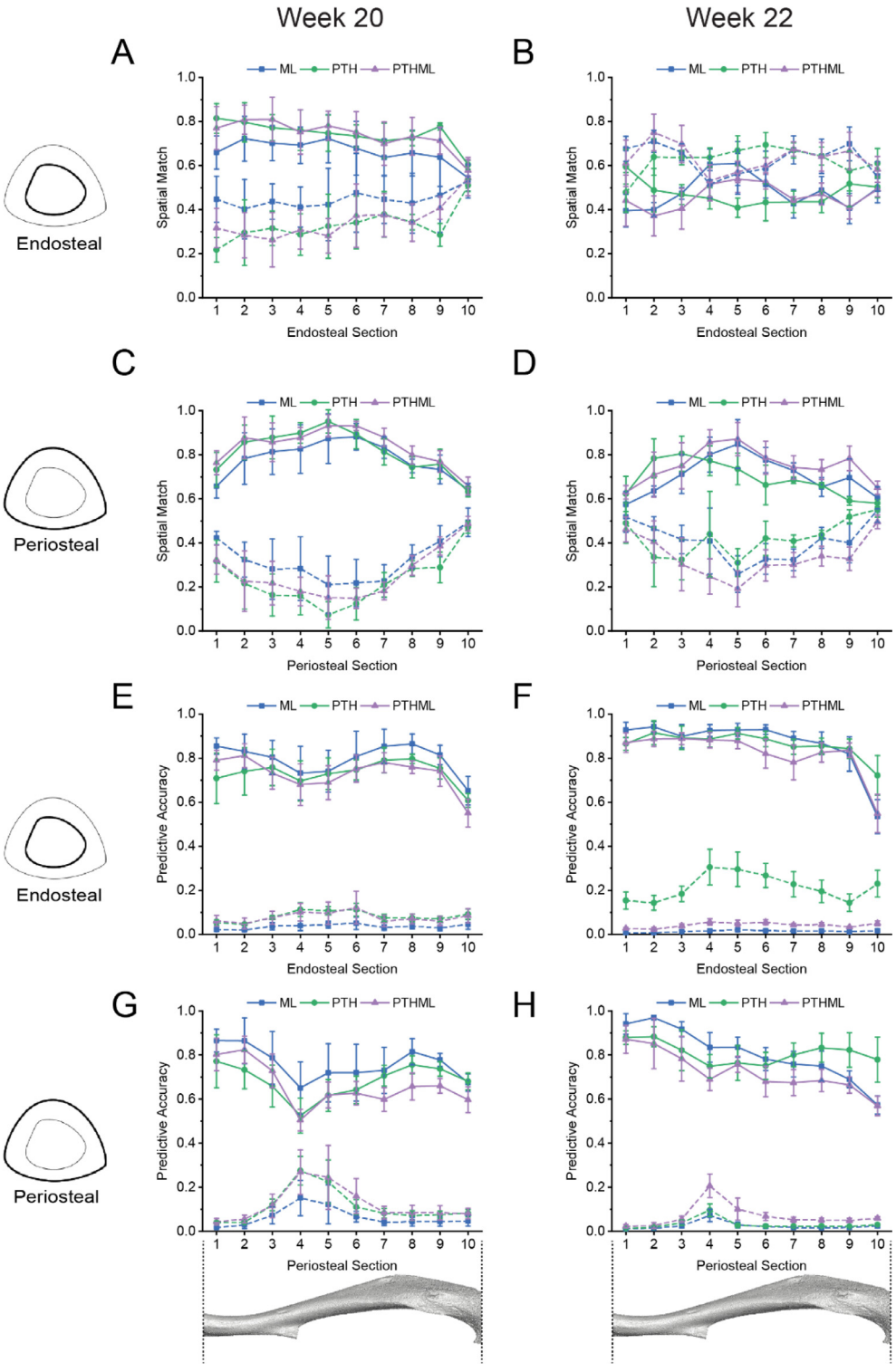

Fig. 8. The extent that bone adaptation is driven by changes in strain at the organ level. Results are separated into spatial match, which is the ratio between the number of correctly predicted voxels and the total predicted voxels of the same type, on the (A-B) endosteal and (C-D) periosteal surfaces; and prediction accuracy, which measures the number of correctly predicted voxels, normalised by the number of experimentally observed changes of the same type, on the endosteal (E-F) and periosteal (G-H) surfaces. Solid lines indicate apposition while dashed lines indicate resorption across the longitudinal axis from distal (1) to proximal (10).

week old mice after 4 weeks of PTH followed by 2 weeks of mechanical loading [11], whereas only additive effects were seen in 19 months old mice with a similar study design [6]. As PTH injection was performed after the completion of mechanical loading rather than before, this may have reduced the combined effects at weeks 18–20, compared to the case where PTH is injected before the commencement of loading, that was found to stimulate bone formation [46,47]. Moreover, the regions benefiting from the positive interactions of PTH and ML on bone adaptation increased from 60% of the tibial length at weeks 18–20 to 90% at weeks 20–22. The catabolic effect of PTH monotherapy increased at weeks 20–22, highlighting the effect of prolonged PTH monotherapy needs to

be carefully managed [11]. Few studies have analysed the effects of interventions on the distal tibia, but we showed for the first time that the additive effects of PTH and mechanical loading in the distal tibia, with PTH improving the BMC and ML contributing to the geometrical properties.

The correlation analyses (Fig. 6) substantiated the capability of the combined experimental-computational approach to understand the contribution of daily physiological loading to bone remodelling in the whole bone. Previous studies have either linked the estimated strains under mechanical loading with the remodelling state to obtain the formation and resorption probability in the whole bone [18,48,49], or directly correlated loading-induced strain and rates of remodelling in small sections of bones through linear regression [10,30]. Our assessment builds on the latter approach but also enables the direct comparison of different treatments. The results showed a strong correlation between the frequency of bone remodelling and the local mechanical environment above the tibiofibular joint at the tissue level (~1 mm), but not below it, for all treated and untreated tibiae. This is consistent with previously published data that showed two different trends in cortical thickness and second moment of area, split at the distal tibio-fibular joint [6,8]. This would explain contradictory results where positive correlations were found in small segments of the mouse tibia [10], but not in rooster tarsometatarsus [50] or turkey radii [51], which have high areal symmetries. The stronger apposition response for the ML and PTHML groups were driven by the increased response in the posterior section, supporting earlier studies that suggested that tensile strain drives higher adaptive response than compressive strain [1].

Predictive models of bone adaptation are useful to understand changes to the bone microarchitecture, fracture risk, and response to treatment [21,25,26,38]. However, predictions of resorption in the mouse tibia using a simple mechanical stimulus have been poor [24,38] or have struggled to predict bone remodelling on the endocortical surfaces [8,42]. In contrast to Frost's mechanostat, results from the murine caudal vertebra [48,49,52] and small segments of the human radius and tibia that showed that resorption increases with decreasing strains, the correlation results in this study showed that resorption in the mouse tibia increased with higher SED under physiological loading. The similar rates of remodelling slopes also suggest that resorption is strongly linked with bone turnover in the mouse tibia under physiological loading. In this study, physiological loading based on the weight of the mice was used to ascertain the effects of all treatments on the bone adaptive response. However, the mismatch in the mechanostat theory and the experimental observation of the resorption envelope was unexpected as the loads applied in the PTH and UNT models were in line with literature [25,26]. Thus, as expected, the use of a mechanostat-based bone remodelling algorithm was only able to predict bone apposition (Fig. 8), even though bone remodelling thresholds for the three treatments have the same trend as the results reported for the murine caudal vertebrae [25]. Most bone remodelling algorithms are centred on the assumption that treatment sensitises bone cells and lowers the set point for remodelling [11,25,26,38,53]. However, the results indicate that the intersections of the correlation analyses were within the same order of magnitude for the UNT, ML and PTH groups, suggesting that the main mechanism for increased bone health is by activating a larger number of sites for bone apposition at locations of higher strains (in the proximal tibia). Finally, the utility of an optimisation algorithm that determines the parameters of bone remodelling by matching the change in shape with time is demonstrated here in the even predictive accuracy in apposition across the tibial length. As a linear bone adaptation algorithm was used, the results also indicate that over 50% of apposition was linearly strain driven.

This work has some limitations that could be overcome in future studies. Firstly, *in vivo* micro-CT imaging is affected by a number of image artefacts (e.g. beam hardening) that may affect the measurements of bone remodelling and changes in densitometric properties. To reduce these effects, we have used an optimised protocol that minimises the effects of radiation on bone remodelling [31] and that includes a beam hardening correction based on high-density wedge shape phantom [35]. Moreover, the changes in densitometric properties were evaluated over a large portion of the bone [36] and with respect to baseline measurements, limiting the effects of artefacts at each time point. Nevertheless, further optimisation of the scanning protocol to increase the image resolution will be needed to provide better estimates of local densitometric properties at the voxel level, which would affect the local geometry in the mechano-regulation models. Secondly, the study design uses a load of 12 N at both time points in the PTH and PTHML groups, matched in peak force to highlight the effects of microstructural and geometrical changes on the response to treatment(s). However, the results showed that bone adaptation (material and geometrical changes) induced after the first set of treatment were different. Therefore, based on the principles of superimposition and sensitivity results of the *in vivo* loading conditions [40], the strains engendered in the mouse tibia at week 21 of loading would be lower in the PTHML group than the ML group. Similarly, all the mice in the PTHML group received 1 week of PTH injections prior to the first application of mechanical loading, hence the applied load of 12 N was not strain-matched across treatment or time. Thus, the effects of mechanical loading with PTH are likely to be under rather than over-estimated. Nevertheless, matching in load improves the translatability of this combined experimental-computational methodology for clinical applications [24] Finally, fluorochrome labelling and immunohistochemistry should be performed as part of future work to determine the role played by osteoblasts and osteoclasts on the resulting bone apposition and resorption at the tissue level.

5. Conclusions

In summary, the use of a validated, multiscale longitudinal micro-CT and micro-FEA combined approach enriches the monitoring and assessment of skeletal health induced by disease and/or treatment, which have previously been limited to mechanical loading or restricted at specific locations. Mechanical loading and PTH treatments as monotherapies or combined therapies showed spatiotemporal differences across groups, additive and non-additive (competitive) interactions between treatments in the proximal and distal tibia. Mechanical loading improved the regulation of bone remodelling to withstand daily physiological load through increased rate of osteogenesis, benefitting primarily the proximal regions, whereas only PTH-based treatments improved bone formation in the distal tibia. Thus, the targeting of bone regions to reduce fracture risk and/or to optimise the dosage and duration of loading and pharmacological interventions will improve the management of osteoporosis. This methodology can be applied to investigate the interactions of other pharmacological treatments, without or with mechanical loading, the mechanisms of skeletal growth and ageing, and potentially for soft tissue development using other imaging modalities.

Data accessibility

The processed data required to reproduce the mechanical loading findings are available to download from doi: 10.15131/shef.data.12927365. Data for the combined treatment has been deposited in Figshare, at doi: 10.15131/shef.data.16685359.

Declaration of Competing Interest

The authors declare that they have no known competing financial interests or personal relationships that could have appeared to influence the work reported in this paper.

Acknowledgements

This work was supported by funding from the Engineering and Physical Sciences Research Council (EPSRC) Frontier Multisim Grant (EP/K03877X/1 and EP/S032940/1) and the National Centre for the Replacement, Refinement and Reduction of Animals in Research (NC3Rs; NC/R001073/1). The authors thank Dr M. Boudiffa, Dr S. Zanjani-Pour, Mr H. Arredondo Carrera, Dr N. Wang, and Prof A. Gartland for help with the acquisition of the data, and Skelet.AL laboratory (http://skeletal.group.shef.ac.uk/) for access to the scanning facilities.

Supplementary materials

Supplementary material associated with this article can be found, in the online version, at doi:10.1016/j.actbio.2021.09.035.

References

[1] J. Wolff, Das Gesetz der Transformation der Knochen, Verlag von August Hirschwald, Berlin, 1892.
[2] W. Roux, Beitrage zur Morphologie der funktionellen Anpassung, Arch. Anat. Physiol. Anat. Abt. (1885) 120–185.
[3] H.M. Frost, Bone “mass” and the “mechanostat”: a proposal, Anat. Rec. 219 (1) (1987) 1–9.
[4] M.E. Chan, G. Uzer, C.T. Rubin, The potential benefits and inherent risks of vibration as a non-drug therapy for the prevention and treatment of osteoporosis, Curr. Osteoporos. Rep. 11 (1) (2013) 36–44.
[5] L. Osagie-Clouard, A. Sanghani, M. Coathup, T. Briggs, M. Bostrom, G.W. Blunn, Parathyroid hormone 1-34 and skeletal anabolic action, Bone Joint Res 6 (1) (2017) 14–21.
[6] L.B. Meakin, H. Todd, P.J. Delisser, G.L. Galea, A. Moustafa, L.E. Lanyon, S.H. Windahl, J.S. Price, Parathyroid hormone’s enhancement of bones’ osteogenic response to loading is affected by ageing in a dose- and time-dependent manner, Bone 98 (2017) 59–67.
[7] A.V. Haas, M.S. LeBoff, Osteoanabolic agents for osteoporosis, J. Endocr. Soc. 2 (8) (2018) 922–932.
[8] A. Carriero, A.F. Pereira, A.J. Wilson, S. Castagno, B. Javaheri, A.A. Pitsillides, M. Marenzana, S.J. Shefelbine, Spatial relationship between bone formation and mechanical stimulus within cortical bone: combining 3D fluorochrome mapping and poroelastic finite element modelling, Bone Rep 8 (2018) 72–80.
[9] J. Eyckmans, C.S. Chen, Making bone via nanoscale kicks, Nat. Biomed. Eng. 1 (9) (2017) 689–690.
[10] A.I. Birkhold, H. Razi, G.N. Duda, S. Checa, B.M. Willie, Tomography-based quantification of regional differences in cortical bone surface remodeling and mechano-response, Calcif. Tissue Int. 100 (3) (2017) 255–270.
[11] T. Sugiyama, L.K. Saxon, G. Zaman, A. Moustafa, A. Sunters, J.S. Price, L.E. Lanyon, Mechanical loading enhances the anabolic effects of intermittent parathyroid hormone (1-34) on trabecular and cortical bone in mice, Bone 43 (2) (2008) 238–248.
[12] M.L. Bouxsein, S.K. Boyd, B.A. Christiansen, R.E. Guldberg, K.J. Jepsen, R. Muller, Guidelines for assessment of bone microstructure in rodents using micro-computed tomography, J. Bone Miner. Res. 25 (7) (2010) 1468–1486.
[13] R. Müller, Long-term prediction of three-dimensional bone architecture in simulations of pre-, peri- and post-menopausal microstructural bone remodeling, Osteoporos. Int. 16 (2005) S25–S35.
[14] M. Aido, M. Kerschnitzki, R. Hoerth, M. Burghammer, C. Montero, S. Checa, P. Fratzl, G.N. Duda, B.M. Willie, W. Wagermaier, Relationship between nanoscale mineral properties and calcein labeling in mineralizing bone surfaces, Connect Tissue Res 55 (Suppl 1) (2014) 15–17.
[15] Y. Lu, M. Boudiffa, E. Dall’Ara, Y. Liu, I. Bellantuono, M. Viceconti, Longitudinal effects of parathyroid hormone treatment on morphological, densitometric and mechanical properties of mouse tibia, J. Mech. Behav. Biomed. Mater. 75 (2017) 244–251.
[16] B.C. Roberts, H.M. Arrendondo Carrera, S. Zanjani-pour, M. Boudiffa, N. Wang, A. Gartland, E. Dall’Ara, PTH(1–34) treatment and/or mechanical loading have different osteogenic effects on the trabecular and cortical bone in the ovariectomized C57BL/6 mouse, Sci. Rep. 10 (2020) 8889.
[17] P. Asgharzadeh, O. Röhrle, B.M. Willie, A.I. Birkhold, Decoding rejuvenating effects of mechanical loading on skeletal aging using in vivo muCT imaging and deep learning, Acta Biomater 106 (2020) 193–207.
[18] B. Javaheri, H. Razi, S. Gohin, S. Wylie, Y. Chang, P. Salmon, P.D. Lee, A.A. Pitsillides, Lasting organ-level bone mechanoadaptation is unrelated to local strain, Sci. Adv. 6 (10) (2020) eaax8301.
[19] M. Viceconti, E. Dall’Ara, From bed to bench: how in silico medicine can help ageing research, Mech. Ageing Dev. 177 (2019) 103–108.
[20] F.M. Lambers, G. Kuhn, F.A. Schulte, K. Koch, R. Müller, Longitudinal assessment of in vivo bone dynamics in a mouse tail model of postmenopausal osteoporosis, Calcif. Tissue Int. 90 (2) (2012) 108–119.
[21] S. Oliviero, M. Giorgi, E. Dall’Ara, Validation of finite element models of the mouse tibia using digital volume correlation, J. Mech. Behav. Biomed. Mater. 86 (2018) 172–184.
[22] S. Oliviero, R. Owen, G.C. Reilly, I. Bellantuono, E. Dall’Ara, Optimization of the failure criterion in micro-Finite Element models of the mouse tibia for the non-invasive prediction of its failure load in preclinical applications, J. Mech. Behav. Biomed. Mater. 113 (2021) 104190.
[23] D. Webster, A. Wirth, G.H. van Lenthe, R. Müller, Experimental and finite element analysis of the mouse caudal vertebrae loading model: prediction of cortical and trabecular bone adaptation, Biomech. Model. Mechanobiol. 11 (1–2) (2012) 221–230.
[24] V.S. Cheong, B.C. Roberts, V. Kadirkamanathan, E. Dall’Ara, Bone remodelling in the mouse tibia is spatio-temporally modulated by oestrogen deficiency and external mechanical loading: a combined in vivo/in silico study, Acta Biomater 116 (2020) 302–317.
[25] A. Levchuk, A. Zwahlen, C. Weigt, F.M. Lambers, S.D. Badilatti, F.A. Schulte, G. Kuhn, R. Müller, The Clinical Biomechanics Award 2012 - presented by the European Society of Biomechanics: large scale simulations of trabecular bone adaptation to loading and treatment, Clin. Biomech. 29 (4) (2014) 355–362.
[26] F.A. Schulte, A. Zwahlen, F.M. Lambers, G. Kuhn, D. Ruffoni, D. Betts, D.J. Webster, R. Müller, Strain-adaptive in silico modeling of bone adaptation–a computer simulation validated by in vivo micro-computed tomography data, Bone 52 (1) (2013) 485–492.
[27] D.C. Tourolle né Betts, E. Wehrle, G.R. Paul, G.A. Kuhn, P. Christen, S. Hofmann, R. Muller, The association between mineralised tissue formation and the mechanical local in vivo environment: time-lapsed quantification of a mouse defect healing model, Sci. Rep. 10 (1) (2020) 1100.
[28] H. Razi, A.I. Birkhold, P. Zaslansky, R. Weinkamer, G.N. Duda, B.M. Willie, S. Checa, Skeletal maturity leads to a reduction in the strain magnitudes induced within the bone: a murine tibia study, Acta Biomater 13 (2015) 301–310.
[29] A.K. Peterson, M. Moody, I. Nakashima, R. Abraham, T.A. Schmidt, D. Rowe, A. Deymier, Effects of acidosis on the structure, composition, and function of adult murine femurs, Acta Biomater 121 (2021) 484–496.
[30] A.I. Birkhold, H. Razi, G.N. Duda, R. Weinkamer, S. Checa, B.M. Willie, The Periosteal Bone Surface is Less Mechano-Responsive than the Endocortical, Sci Rep 6 (2016) 23480.
[31] S. Oliviero, M. Giorgi, P.J. Laud, E. Dall’Ara, Effect of repeated in vivo microCT imaging on the properties of the mouse tibia, PLoS ONE 14 (11) (2019) e0225127.
[32] S. Oliviero, Y. Lu, M. Viceconti, E. Dall’Ara, Effect of integration time on the morphometric, densitometric and mechanical properties of the mouse tibia, J. Biomech. 65 (2017) 203–211.
[33] R.L. de Souza, M. Matsuura, F. Eckstein, S.C. Rawlinson, L.E. Lanyon, A.A. Pitsillides, Non-invasive axial loading of mouse tibiae increases cortical bone formation and modifies trabecular organization: a new model to study cortical and cancellous compartments in a single loaded element, Bone 37 (6) (2005) 810–818.
[34] B.C. Roberts, M. Giorgi, S. Oliviero, N. Wang, M. Boudiffa, E. Dall’Ara, The longitudinal effects of ovariectomy on the morphometric, densitometric and mechanical properties in the murine tibia: a comparison between two mouse strains, Bone 127 (2019) 260–270.
[35] G.J. Kazakia, A.J. Burghardt, S. Cheung, S. Majumdar, Assessment of bone tissue mineralization by conventional x-ray microcomputed tomography: comparison with synchrotron radiation microcomputed tomography and ash measurements, Med. Phys. 35 (7) (2008) 3170–3179.
[36] Y. Lu, M. Boudiffa, E. Dall’Ara, I. Bellantuono, M. Viceconti, Development of a protocol to quantify local bone adaptation over space and time: quantification of reproducibility, J. Biomech. 49 (10) (2016) 2095–2099.
[37] S. Oliviero, M. Roberts, R. Owen, G.C. Reilly, I. Bellantuono, E. Dall’Ara, Non-invasive prediction of the mouse tibia mechanical properties from microCT images: comparison between different finite element models, Biomech. Model Mechanobiol. (2021).
[38] V.S. Cheong, A. Campos Marin, D. Lacroix, E. Dall’Ara, A novel algorithm to predict bone changes in the mouse tibia properties under physiological conditions, Biomech. Model Mechanobiol. 19 (2020) 985–1001.
[39] J.P. Charles, O. Cappellari, J.R. Hutchinson, A dynamic simulation of musculoskeletal function in the mouse hindlimb during trotting locomotion, Front. Bioeng. Biotechnol. 6 (2018) 61.
[40] V.S. Cheong, V. Kadirkamanathan, E. Dall’Ara, The Role of the Loading Condition in Predictions of Bone Adaptation in a Mouse Tibial Loading Model, Front. Bioeng. Biotechnol. 9 (2021) 676867.
[41] R.P. Main, S.J. Shefelbine, L.B. Meakin, M.J. Silva, M.C.H. van der Meulen, B.M. Willie, Murine axial compression tibial loading model to study bone mechanobiology: implementing the model and reporting results, J. Orthop. Res. 38 (2) (2020) 233–252.
[42] A.F. Pereira, B. Javaheri, A.A. Pitsillides, S.J. Shefelbine, Predicting cortical bone adaptation to axial loading in the mouse tibia, J. R. Soc. Interface 12 (110) (2015) 0590.
[43] R.L. Jilka, M. Almeida, E. Ambrogini, L. Han, P.K. Roberson, R.S. Weinstein, S.C. Manolagas, Decreased oxidative stress and greater bone anabolism in the

aged, when compared to the young, murine skeleton with parathyroid hormone administration, Aging Cell 9 (5) (2010) 851–867.
[44] E. Canalis, A. Giustina, J.P. Bilezikian, Mechanisms of anabolic therapies for osteoporosis, N. Engl. J. Med. 357 (9) (2007) 905–916.
[45] M. Rubin, F. Cosman, R. Lindsay, J. Bilezikian, The anabolic effects of parathyroid hormone, Osteoporos. Int. 13 (4) (2002).
[46] S. Brunner, H.D. Theiss, A. Murr, T. Negele, W.M. Franz, Primary hyperparathyroidism is associated with increased circulating bone marrow-derived progenitor cells, Am. J. Physiol. Endocrinol. Metab. 293 (6) (2007) E1670–E1675.
[47] S. Brunner, M.M. Zaruba, B. Huber, R. David, M. Vallaster, G. Assmann, J. Mueller-Hoecker, W.M. Franz, Parathyroid hormone effectively induces mobilization of progenitor cells without depletion of bone marrow, Exp. Hematol. 36 (9) (2008) 1157–1166.
[48] A. Malhotra, M. Walle, G.R. Paul, G.A. Kuhn, R. Muller, Application of subject-specific adaptive mechanical loading for bone healing in a mouse tail vertebral defect, Sci. Rep. 11 (1) (2021) 1861.
[49] A.C. Scheuren, P. Vallaster, G.A. Kuhn, G.R. Paul, A. Malhotra, Y. Kameo, R. Muller, Mechano-regulation of trabecular bone adaptation Is controlled by the local in vivo environment and logarithmically dependent on loading frequency, Front. Bioeng. Biotechnol. 8 (2020) 566346.
[50] S. Judex, T.S. Gross, R.F. Zernicke, Strain gradients correlate with sites of exercise-induced bone-forming surfaces in the adult skeleton, J. Bone Miner. Res. 12 (10) (1997) 1737–1745.
[51] T.S. Gross, J.L. Edwards, K.J. Mcleod, C.T. Rubin, Strain gradients correlate with sites of periosteal bone formation, J. Bone Miner. Res. 12 (6) (1997) 982–988.
[52] Z. Li, D. Betts, G. Kuhn, M. Schirmer, R. Müller, D. Ruffoni, Mechanical regulation of bone formation and resorption around implants in a mouse model of osteopenic bone, J. R. Soc. Interface 16 (152) (2019) 20180667.
[53] V.S. Cheong, P. Fromme, A. Mumith, M.J. Coathup, G.W. Blunn, Novel adaptive finite element algorithms to predict bone ingrowth in additive manufactured porous implants, J. Mech. Behav. Biomed. Mater. 87 (2018) 230–239.